

Visual Learning-based Planning for Continuous High-Dimensional POMDPs

Sampada Deglurkar,^{1,*} Michael H. Lim,^{1,*} Johnathan Tucker,²
Zachary N. Sunberg,² Aleksandra Faust,³ Claire J. Tomlin¹

¹Department of Electrical Engineering and Computer Sciences, UC Berkeley

²Department of Aerospace Engineering Science, CU Boulder

³Google Research

Abstract

The Partially Observable Markov Decision Process (POMDP) is a powerful framework for capturing decision-making problems that involve state and transition uncertainty. However, most current POMDP planners cannot effectively handle very high-dimensional observations they often encounter in the real world (e.g. image observations in robotic domains). In this work, we propose Visual Tree Search (VTS), a learning and planning procedure that combines generative models learned offline with online model-based POMDP planning. VTS bridges offline model training and online planning by utilizing a set of deep generative observation models to predict and evaluate the likelihood of image observations in a Monte Carlo tree search planner. We show that VTS is robust to different observation noises and, since it utilizes online, model-based planning, can adapt to different reward structures without the need to re-train. This new approach outperforms a baseline state-of-the-art on-policy planning algorithm while using significantly less offline training time.

1 Introduction

Many real world sequential decision problems that involve uncertainty, such as autonomous driving (Bai et al. 2015; Sunberg, Ho, and Kochenderfer 2017), cancer screening (Ayer, Alagoz, and Stout 2012), spoken dialog systems (Young et al. 2013), and aircraft collision avoidance (Holland, Kochenderfer, and Olson 2013) can be expressed and solved using the partially observable Markov decision process (POMDP) formalism. A POMDP is an optimization problem in which we aim to find a policy that maps states to actions which will control the state to maximize the expected sum of rewards. Finding an optimal POMDP policy is computationally demanding, and often intractable, due to the uncertainty introduced by imperfect observations (Papadimitriou and Tsitsiklis 1987). One popular approach to deal with this computational challenge is to use *online* algorithms that look for local approximate policies as the agent interacts with the environment rather than computing a global policy that maps every possible outcome to an action.

Many online POMDP algorithms are variants of Monte Carlo tree search (MCTS) (Browne et al. 2012; Silver and

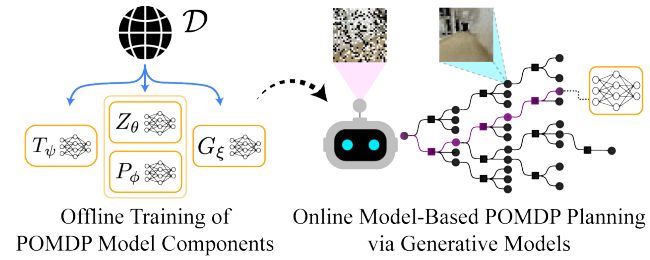


Figure 1: Visual Tree Search uses generative models to interface offline generative model training and online model-based POMDP filtering and planning.

Veness 2010; Sunberg and Kochenderfer 2018) or other tree search variants (Ye et al. 2017; Kurniawati and Yadav 2016). These state-of-the-art algorithms for continuous POMDPs are shown to be computationally efficient (Sunberg and Kochenderfer 2018; Mern et al. 2021; Lim, Tomlin, and Sunberg 2021) and proven to have finite sample convergence guarantees to the optimal policy (Lim, Tomlin, and Sunberg 2020, 2021), which make them desirable candidates for planning. However, these methods rely on having access to a known generative model, which limits the class of problems they can solve in practice. Thus, in many realistic scenarios with high dimensional observations like RGB images, tree search methods cannot be applied without knowing or learning the relevant models or simplifying the environment.

One alternative approach is to train a model-free deep neural network policy to learn both a latent belief representation and a planner (Karkus, Hsu, and Lee 2017; Mnih et al. 2013; Igl et al. 2018). These model-free approaches benefit from not having to specify the spaces and models and being able to learn complex policies. However, they may not generalize well to new unseen tasks, their models lack interpretability, and they do not leverage much prior knowledge about the system, especially in robotics settings.

On the other hand, model-based approaches, such as Differentiable Particle Filters (DPF) (Jonschkowski, Rastogi, and Brock 2018) and Dual Sequential Monte Carlo (DualSMC) (Wang et al. 2020) that we build off of in this work, combine classical filtering and planning techniques with deep learning. Introducing an algorithmic prior allows each model to focus on a specific task, making them sample

*These authors contributed equally.

Copyright © 2022, Association for the Advancement of Artificial Intelligence (www.aaai.org). All rights reserved.

efficient and robust. Furthermore, the classical techniques that are integrated with neural networks often come with theoretical guarantees and are interpretable. These methods, however, rely on simplified approaches for planning in the belief space, not fully accounting for the uncertainty.

Recently, compositional learning approaches have increased interest in identifying suitable algorithmic priors for intelligent planning with minimal training. Compositional learning methods allow agents to capture complex relations given limited data (Andreas et al. 2016; Hudson and Manning 2018; Kirsch, Kunze, and Barber 2018). Moreover, compositional reinforcement learning methods allow algorithmic priors for autonomous agents (Devin et al. 2017; Yang et al. 2020; Mittal et al. 2020).

Our key insight is to bring compositional approaches into realistic POMDP problems by bridging offline training of individual sets of models and online model-based planning with such learning-enabled components. We believe that solving such reinforcement learning problems with composition of generative models trained by unsupervised learning instead can result in more data efficient and robust learning and planning. Fig. 1 shows the overview of our approach.

Our contributions in this work are as follows:

- We propose Visual Tree Search (VTS), a procedure to solve continuous high-dimensional POMDPs in two steps. First, we learn a set of generative models that represent the different POMDP model components, effectively framing the POMDP problem as a compositional learning problem. Second, we use these learned models to interface the two model-based techniques: particle filtering and online POMDP planning.
- We claim that conditional generative models are sufficient to enable planning with high dimensional observations. Specifically, we show that generating images using Conditional Variational Autoencoders (CVAEs) (Sohn, Lee, and Yan 2015) in conjunction with particle generative models from DualSMC allow effective planning.
- We perform empirical analyses based on experiments inspired by Wang et al. (2020), which demonstrate not only that VTS outperforms a baseline state-of-the-art on-policy planning algorithm, but also that the compositional training procedure enhances performance, robustness, and interpretability of neural network components.

2 Background

POMDPs. A POMDP is defined with a 7-tuple $(S, A, O, T, Z, R, \gamma)$, with state space S , action space A , observation space O , transition density $T(s'|s, a)$, observation density $Z(o|s)$, reward function $R(s, a)$, and discount $\gamma \in [0, 1]$ (Kochenderfer 2015; Bertsekas 2005). Specifically, we use the phrase “continuous POMDP” to denote those with continuous state, action and observation spaces. For POMDPs, since the agent receives only noisy observations of the true state, the agent can infer the state by maintaining a belief $b_t \in B$ at each step t and updating it with new action and observation pair (a_{t+1}, o_{t+1}) via Bayesian filtering (Kaelbling, Littman, and Cassandra 1998). For our neural network training procedures, we

make the ground truth state information available to the planner, but keep them unavailable during testing. A policy $\pi : B \rightarrow A$ maps a belief b to an action a . To solve a POMDP problem, the agent seeks to find an optimal policy π^* that maximizes the expected cumulative reward.

Monte Carlo Tree Search. In Monte Carlo planning, it is not always necessary to explicitly evaluate the probability density of the transition or observation distributions, and merely generating samples of next state s' , reward r , and observation o is sufficient. In particular, many Monte Carlo Tree Search (MCTS) algorithms only require that we have a generative model G that can generate (s', r, o) samples, where we can sample $s' \sim T(s'|s, a)$ and $o \sim Z(o|s')$ according to their correct densities. Using these generative models, the MCTS methods reason about the transition and observation densities via sampling to approximate the true reward distribution by balancing exploration and exploitation, and subsequently find an approximate online policy that maximizes the expected sum of rewards at each planning step.

Conditional generative models. Many models in deep learning are used to approximate probability distributions. However, *sampling* from these distributions requires a different class of models referred to as generative models. While some types of generative models, such as Generative Adversarial Networks (GANs), try to sample from distributions by making the samples seem as “realistic” as possible, other models such as Variational Autoencoders (VAEs) map complex distributions into simpler ones via latent space embedding. *Conditional* generative models condition on another variable to sample from conditional distributions; in our work, we use conditional generative models G to sample observations conditioned on the agent state, and P to propose state particles given the current observation.

3 Related Works

Planning under uncertainty. Recently, state-of-the-art MCTS approaches have shown success in relatively large or continuous space POMDP planning problems. Most notably, POMCPOW and PFT-DPW (Sunberg and Kochenderfer 2018), LABECOP (Hoerger and Kurniawati 2020), and DESPOT- α (Garg, Hsu, and Lee 2019) were shown to be effective in solving continuous observation POMDP problems. They use weighted collections of particles to efficiently represent complex beliefs. Provided the particles are weighted appropriately based on the observation likelihood, tree search using these particle beliefs will converge to a globally optimal policy (Lim, Tomlin, and Sunberg 2020). Furthermore, these works led to planners that can solve fully continuous or even hybrid space POMDP problems, using techniques such as continuous bandits (Lim, Tomlin, and Sunberg 2021) or Bayesian optimization (Mern et al. 2021). These tree search methods require knowing Z, T, G models to effectively plan, which we aim to learn with neural networks to extend the scope of the tree search methods. In this work, we integrate the PFT-DPW algorithm to handle learning-based model components.

Deep reinforcement learning solvers. Model-free deep reinforcement learning solvers train a neural network policy to learn both a latent belief representation, usually in tensor form, as well as a planner using that representation. For instance, Deep Q-Network (Mnih et al. 2013) learns a Q -value-based planner in the complex state and action space, and more recent approaches like QMDP-net (Karkus, Hsu, and Lee 2017), and Deep Variational Reinforcement Learning (Igl et al. 2018) maintain a latent belief vector whose update rule is also learned via a neural network. This latent belief representation is then used as an input to learn a value function and policy.

Differentiable particle filters. Model-based deep learning solvers for POMDP problems attempt to combine classical filtering and planning techniques with deep learning. One such successful framework is Differentiable Particle Filter (DPF) (Jonschkowski, Rastogi, and Brock 2018), which allows conventional particle filtering techniques to be interfaced with complex visual observations. This algorithm contains multiple linked neural network components, including a particle proposer, an observation model and a dynamics model, that are designed to be trained end-to-end. A recent work extends DPF with entropy regularization and provides convergence guarantees (Corenflos et al. 2021).

Dual Sequential Monte Carlo (DualSMC) (Wang et al. 2020) extends this method further to introduce an adversarial filtering objective and integrate in the SMC planner, making it a fully closed-loop POMDP solver. The SMC planner rolls out learned policies from a set of weighted state particles that approximate a belief state, but without considering future observation sequences. Such approximation effectively assumes that the state uncertainty vanishes at the next step, which is proven to be sometimes suboptimal (Kaelbling, Littman, and Cassandra 1998). In this work, we extend DPF and DualSMC to interface tree search planners.

Compositional learning. Compositional learning aims to break down neural network components, such that different components can specialize in different tasks and be integrated to learn complex relations with little data and training. Such compositional learning can be achieved either through provided compositional structure in the form of an algorithmic prior (Andreas et al. 2016; Hudson and Manning 2018), or by automatically discovering such structures (Rosenbaum, Klinger, and Riemer 2018; Alet, Lozano-Perez, and Kaelbling 2018; Kirsch, Kunze, and Barber 2018; Meyerson and Miikkulainen 2018). Furthermore, compositional learning methods have been applied to various reinforcement learning settings (Devin et al. 2017; Yang et al. 2020; Mittal et al. 2020), in which the agent is comprised of neural networks designed for autonomous learning and planning. Another approach uses generative models and recurrent networks to learn different representations of the environment (Ha and Schmidhuber 2018).

4 Visual Tree Search

Solving a POMDP can be split into filtering and planning problems. In the Visual Tree Search (VTS) algorithm, we

aim to integrate the learned POMDP model components with classical planning and filtering techniques. This results in a POMDP solver that can learn model components that are both sample efficient and more interpretable than end-to-end approaches. It also benefits from having a robust particle filter and planner built upon techniques with theoretical guarantees, and can adapt to different task rewards. To integrate sampling-based online tree search planner techniques, we must have access to a generative model that can generate image observations o from a given state s according to the likelihood density $Z(o|s)$. In this section, we outline the filtering and planning algorithms and models, and the corresponding compositional training procedure. Fig. 2 and Algorithm 1 outline the VTS algorithm.

4.1 Differentiable Particle Filtering

For particle filtering, we can utilize a family of architectures called Differentiable Particle Filtering (DPF) (Jonschkowski, Rastogi, and Brock 2018), which combine classical particle filtering algorithms with convolutional neural networks that can handle complex observations. For this filtering procedure, we learn two neural network-based models: (1) Observation density Z_θ , (2) Particle proposer P_ϕ :

$$w_t = Z_\theta(o_t|s_t), \quad (1)$$

$$s_t \sim P_\phi(o_t). \quad (2)$$

The Greek letters denote the parameters of these neural network models. Specifically for our work, we use the DPF architecture introduced in DualSMC (Wang et al. 2020), where the observation and proposer networks are trained with an adversarial optimization objective. In principle, we can also train DPF with entropy regularization (Corenflos et al. 2021) with optimality guarantees. We assume that the transition model T is known, which is not a limiting assumption for many POMDP problems (e.g. POMDPs with physical dynamics), but in principle it can be learned and modeled with a neural network T_ψ as well.

The filtering procedure is described below, where the belief is represented by $b_t \approx \{s_t^{(k)}, w_t^{(k)}\}_{k=1}^K$. First, the agent takes a step with an action chosen by the tree search planner. Then, the agent updates the predicted states $(s'_{t+1})^{(k)}$ with the transition model T . The observation o_t obtained from the environment is fed into the observation density Z_θ , which provides the likelihood of an observation given the state. This in turn is used to update the likelihood weights $(w'_{t+1})^{(k)}$ of each particle. In order to ensure robustness in the particle representation of the belief state, the particle proposer generative model P_ϕ proposes plausible state particles for a given observation, replacing some fraction of the particles. This fraction is fixed in our experiments, but it can be made to decay exponentially over time (Wang et al. 2020).

4.2 Tree Search Planner

Monte Carlo Tree Search. For the online planner, we use the Particle Filter Trees-Double Progressive Widening (PFT-DPW) algorithm (Sunberg and Kochenderfer 2018). PFT-DPW is a particle belief-based MCTS planner, and it is chosen due to its relative ease of implementation and vectorization of particle filter algorithms. Also, it is proven that the

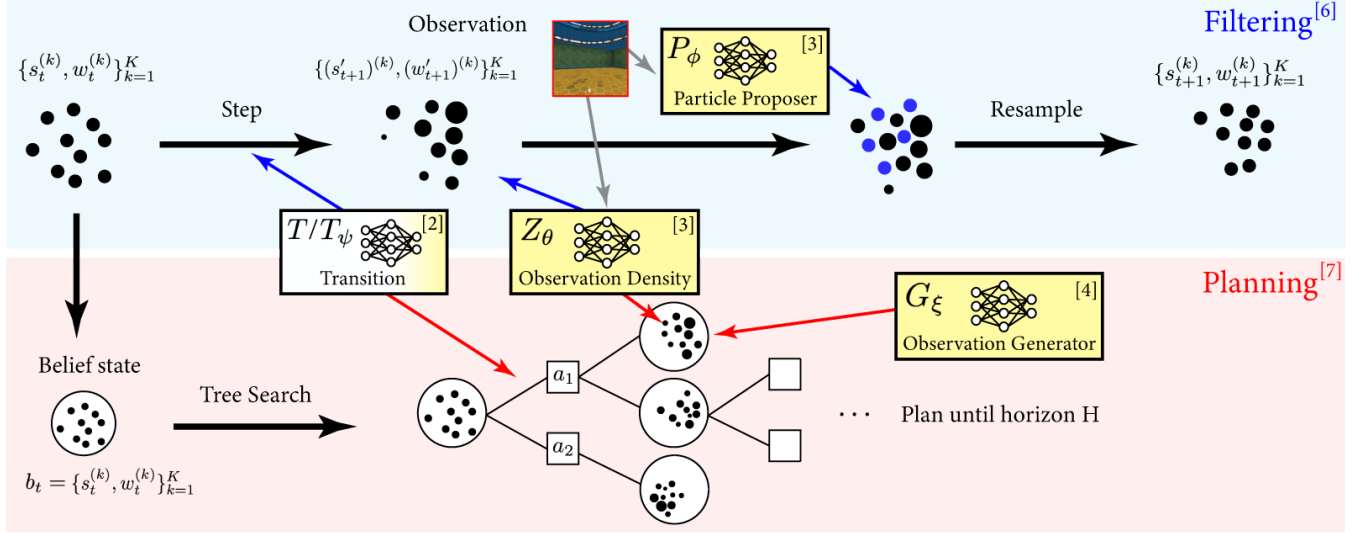


Figure 2: Overview of the Visual Tree Search (VTS) system. The models learned with neural networks are shown in yellow – transition model is colored with a gradient, since it can be learned or pre-defined. The contributions of the models for filtering are shown in blue arrows, and planning in red arrows, and numbers in brackets show corresponding steps in Algorithm 1.

simplified version of PFT-DPW has optimality guarantees (Lim, Tomlin, and Sunberg 2020). However, any continuous POMDP tree search planner can be used instead.

For our navigation problems, we discretize the action space such that the robotic agent moves in the 8 cardinal and diagonal directions with full thrust. While this means we work with a limited action space, we can ensure that we travel with full thrust to get to the goal faster and reduce the complexity of both planning and generating observations. Furthermore, we provide PFT-DPW with a naïve rollout policy of actuating straight towards the goal and calculating the expected reward, which PFT-DPW can use as a reference and vastly improve upon.

Observation generative model. We claim that generative models enable online model-based POMDP planning with images. To plan with a tree search planner, we need to be able to generate the next step states and observations, as well as evaluate the likelihood of the observations. With models from DPF, we can generate the next step state with transition model T and calculate the likelihood weight with observation density $Z_θ$, which are also used in the filtering procedure. Thus, we only additionally need to learn a generative model $G_ξ$ that generates an observation o_t given a state s_t :

$$o_t \sim G_ξ(s_t). \quad (3)$$

We use a Conditional Variational Autoencoder (CVAE) (Sohn, Lee, and Yan 2015) to model the observation generator $G_ξ$. We denote the encoder neural network as $E(s_t, o_t)$ and the decoder as $\hat{D}(s_t, z)$, where the state s_t is the conditional variable. The encoder outputs a normal distribution with mean $μ$ and standard deviation $σ$, and z is sampled from this distribution. Letting $p_{\hat{D}}(o_t|s_t, z)$ and $p_E(z|o_t, s_t)$ represent the distributions characterized by the decoder and

Algorithm 1: Visual Tree Search Algorithm.

Input: Hyperparameters for neural networks ($ζ$), DPF ($χ$), MCTS ($ρ$), maximum time step T_{max} .

Output: Action a_t at each step t .

- 1: Collect data $ℳ$ of tuples (s_t, a_t, o_t, s_{t+1}) , either through random sampling or exploration of the environment.
- 2: [Optional] Train the transition model $T_ψ$ with data tuples (s_t, a_t, s_{t+1}) .
- 3: [DualSMC] Jointly train the observation density model $Z_θ$ and particle proposer model $P_φ$ with data tuples $(s_t, o_t, \{s_{t,i}\})$, where $\{s_{t,i}\}$ are particle estimates of s_t .
- 4: [CVAE] Train the observation generator model $G_ξ$ with data tuples (s_t, o_t) .
- 5: **for** $t = 1$ to T_{max} **do**
- 6: **[DualSMC]** If $t = 1$, initialize the belief state b_t . Otherwise, after receiving o_t , update the belief state b_t with $DPF(T_ψ, Z_θ, P_φ, χ)$.
- 7: **[PFT-DPW]** Run MCTS($T_ψ, Z_θ, G_ξ, ρ$) on the belief state b_t to obtain action a_t and take the action.
- 8: **end for**

*Algorithm components/architecture adapted from other works shown in brackets: [yellow] denotes training, [blue] filtering, and [red] planning.

encoder respectively, we have the standard ELBO loss

$$\begin{aligned} \mathcal{L}(o_t, s_t) = & -\mathbb{E}_{o_t} [\log(p_{\hat{D}}(o_t|s_t, z))] \\ & + \text{KL}(p_E(z|o_t, s_t)||p(z|s_t)), \end{aligned} \quad (4)$$

where $p(z|s_t)$ is a unit normal prior. While there are other conditional generative models such as Conditional Generative Adversarial Network (CGAN) (Mirza and Osindero 2014), we noticed the most consistent performance and easiest training from the CVAE for our experiments.

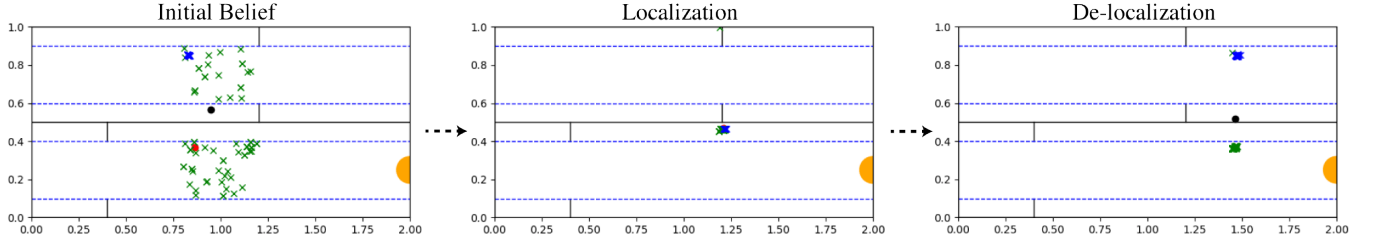


Figure 3: Example particle filtering performance when de-localization occurs. Planner starts with an initial distribution of states (left), then localizes in the wall states (middle), but sometimes loses the localization after exiting the wall states (right). Red dot indicates true state, black dot the mean belief state, green crosses the belief particles, and blue crosses the proposed particles.

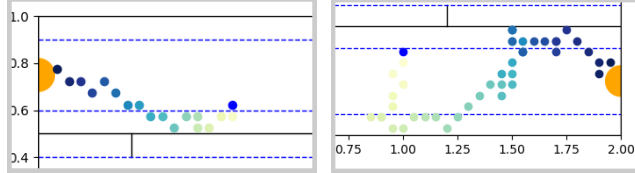


Figure 4: Example trajectories taken by the VTS solver: VTS typically quickly localizes and reaches the goal (left), but in a few cases it takes a lengthy detour (right).

4.3 Compositional Training of Visual Tree Search

To train the neural network models, we employ a training procedure for each of the models with pre-collected data \mathcal{D} , which contain tuples of (s_t, a_t, o_t, s_{t+1}) . Lines 1-4 of Algorithm 1 outline the training procedure. We provide the Z_θ and P_ϕ models with randomly sampled batches of state, observation and synthetic belief particle sets: $(s_t, o_t, \{\hat{s}_{t,i}\})$. While the belief particle sets are not a part of the pre-collected data, we can easily generate them by sampling states from a normal distribution centered at s_t . The Z_θ and P_ϕ are trained with the adversarial objective in DualSMC (Wang et al. 2020): Z_θ serves as a discriminator that gives higher likelihoods to states that are more likely for a given observation, and P_ϕ serves as a generator that proposes plausible state particles for a given observation. The G_ξ model is trained with random batches of samples of state and observation pairs: (s_t, o_t) . These random batches provide a good data prior for all types of states and observations an agent may encounter during planning, unlike DualSMC which only encounters states and observations from acting according to the locally optimal policy.

Compared to other on-policy RL algorithms and architectures, the VTS training procedure shifts the POMDP problem from a reinforcement learning problem to a compositional learning problem, in which training each model in the POMDP is framed as an unsupervised learning problem. This drastically decreases the problem complexity, as we have explicit control over what each model is learning and the schedule of the training. It also allows us to better approximate the data distribution via sampling or exploration, as opposed to an evolving on-policy planner distribution that often starts off poorly and provides heavily biased data.

Technically, we could employ additional on-policy learn-

ing to refine the networks to focus on parts of the problem that are relevant for a given task as done in training DPF-based policies (Jonschkowski, Rastogi, and Brock 2018). However, we found that on-policy learning does not significantly improve performance in addition to regular training, since the planner often successfully and quickly reaches the goal and does not provide many new samples in areas where the models need improvement.

5 Experiments

Our experiments mirror the experiments done in (Wang et al. 2020). First, we tested our algorithm on the 2D Floor Positioning problem to demonstrate that using the VTS learning and planning procedure can significantly cut down the training time to learn a solver that is agnostic to the task or reward structure of the problem. Then, we prepared our own version of the 3D Light-Dark problem in the Stanford 3D dataset (Armeni et al. 2017) to set up a more challenging navigation task that requires the agent to plan with realistic indoor building RGB images. The hyperparameters and computation details are given in Appendix A.

5.1 Floor Positioning Problem

In this problem, a robotic agent is randomly placed around the center of either the top or the bottom floor. However, the agent does not know its ground truth state position, and must infer its position by relying on a radar-like observation in all four cardinal directions, which bounces off the nearest wall. The top and bottom floors are indistinguishable within the ‘‘corridor states’’ of the hallways, but the robotic agent can take advantage of the ‘‘wall states’’ by traveling closer to the top or bottom walls of each floor, where it can receive different observations due to the different wall placements in each floor. The agent must reach the goal and avoid the trap, where the goal is the left end of the hallway in the top floor and right end in the bottom floor, and the trap is at the opposite side of the goal in each floor.

To train the Z_θ , P_ϕ , and G_ξ models, we employed the following procedure. Z_θ and P_ϕ were provided with random batches of samples $(s_t, o_t, \{\hat{s}_{t,i}\})$, with $s_t = (x_t, y_t)$ being the agent’s position. The $\{\hat{s}_{t,i}\}$ were generated from a normal distribution centered at s_t with standard deviation 0.01. G_ξ was provided with random batches of samples (s_t, o_t) , where for each batch we sampled the s_t and generated each o_t from

Table 1: Summary of planner performances on the Floor Positioning problem and the 3D Light-Dark problem variants. Each column reports the mean of means estimator over different seeds: 5 for Floor Positioning, 3 for 3D Light-Dark, and \pm indicates one standard error of the estimator. Mean particle distance is defined as the mean of the distance between the mean belief state and the true state. All statistics are for when the agent is successful.

Planner & Problem	Mean Task Success (%)	Mean Reward	Mean Steps Taken	Training Time (h)	Planning Time (s)	Mean Particle Distance
Floor Positioning						
VTS (Ours)	97.4 \pm 0.007	99.84 \pm 0.11	33.92 \pm 0.96	8.77 \pm 0.02	0.29 \pm 0.002	0.09 \pm 0.005
DualSMC	99.0 \pm 0.005	100.0 \pm 0.0	25.55 \pm 0.10	14.14 \pm 0.58	0.05 \pm 0.004	0.09 \pm 0.002
[From (Wang et al. 2020)]						
Adversarial PF + SMCP	95.0	–	73.3	–	–	–
DVRL	38.3	–	162.0	–	–	–
3D Light-Dark						
VTS (Ours)	100 \pm 0.0	99.27 \pm 0.52	17.28 \pm 1.32	9.03 \pm 0.2	0.80 \pm 0.004	0.33 \pm 0.02
DualSMC	99.9 \pm 0.001	97.67 \pm 1.66	24.05 \pm 0.74	12.49 \pm 0.97	0.06 \pm 0.001	0.46 \pm 0.04
3D Light-Dark + Traps						
VTS (Ours)	97.3 \pm 0.004	85.12 \pm 7.71	25.83 \pm 1.97	–	1.23 \pm 0.02	0.29 \pm 0.02
DualSMC	99.9 \pm 0.001	–24.37 \pm 2.62	24.1 \pm 1.09	–	0.06 \pm 0.0005	0.46 \pm 0.03
3D Light-Dark + Occlusions						
VTS (Ours)	99.3 \pm 0.005	93.98 \pm 3.05	32.23 \pm 5.32	–	0.87 \pm 0.06	0.73 \pm 0.08
DualSMC	80.2 \pm 0.1	17.33 \pm 9.59	46.26 \pm 3.94	–	0.06 \pm 0.001	0.83 \pm 0.03

the corresponding s_t . The sampling procedure for the states was biased towards the wall states, since those states were more difficult to learn from. That is, for Z_θ and P_ϕ , in each batch a state would be chosen from a wall with 0.5 probability and from anywhere in the environment with 0.5 probability. For G_ξ , in each batch a state would be chosen from a wall with 0.5 probability, from a non-wall area with 0.375 probability, and from anywhere else with 0.125 probability.

Planner comparison. We show the results of the planner performances in Table 1 for 1000 testing episodes. We evaluated the planners – VTS and DualSMC – and collected the results. We also include the results from the other two planners, Adversarial PF + SMCP and DVRL, which are directly taken from Wang et al. (Wang et al. 2020) for reference. We note that VTS and DualSMC both have very high success rates. We also tested DualSMC with a known T model to ensure VTS is not given an advantage by knowing T , but observed no statistically significant difference in performance.

Overall, we note that VTS plans reasonably fast with an online planner that is quicker to train and agnostic to the reward at hand, though it performs slightly worse than DualSMC in the Floor Positioning problem. We see that DualSMC takes the least amount of steps, taking an average of 25.55 steps to reach the goal, whereas VTS takes around 8 more steps on average than DualSMC. In Fig. 4, we see that while the VTS solver is quick to localize and then reach the goal, it sometimes needs to re-localize and take a detour. This is mostly due to the fact that VTS does not use an LSTM as one of the intermediate layers in Z_θ because Z_θ is trained offline from randomly collected data. This results in particle de-localization, as the observation density cannot propagate forward the localized information.

Fortunately, this is not a challenging problem to solve, and there are many potential methods to overcome this problem, such as exponentially decaying the number of particles replaced (Wang et al. 2020) or only proposing particles when a particle deficiency has been detected (Gustafsson 2010). Even so, the VTS planner reaches the goal in a reasonable number of steps in line with DualSMC, especially in comparison with the other two solvers that either take large amounts of steps or fail frequently.

We also see a large difference between VTS and DualSMC in the training and planning times. The VTS training procedure only takes around 8.77 hours, while DualSMC on-policy training takes around 14.14 hours, which means VTS training is nearly twice as fast. The VTS training does not rely on planner performance, as it just needs to be supplied with relevant state and observation batches. However, DualSMC on-policy training requires the policy to interact with the environment, and as such, much of the time is spent earlier in the training episodes when the planner can neither localize nor reach the goal.

For online planning speed, VTS takes around 0.29 seconds to plan on average while DualSMC only requires 0.05 seconds, which means VTS planning is 5-6 times slower. Since tree search methods learn the policy online and are more difficult to parallelize, they typically trade off the offline training time with the online learning and planning time. Despite the longer planning, VTS plans reasonably fast while maintaining the flexibility of an online planner.

5.2 3D Light-Dark Problem

The Light-Dark problem is a family of problems in which an agent is tasked to localize in the “light” region before reaching the goal in the “dark” region, and the agent receives noise-

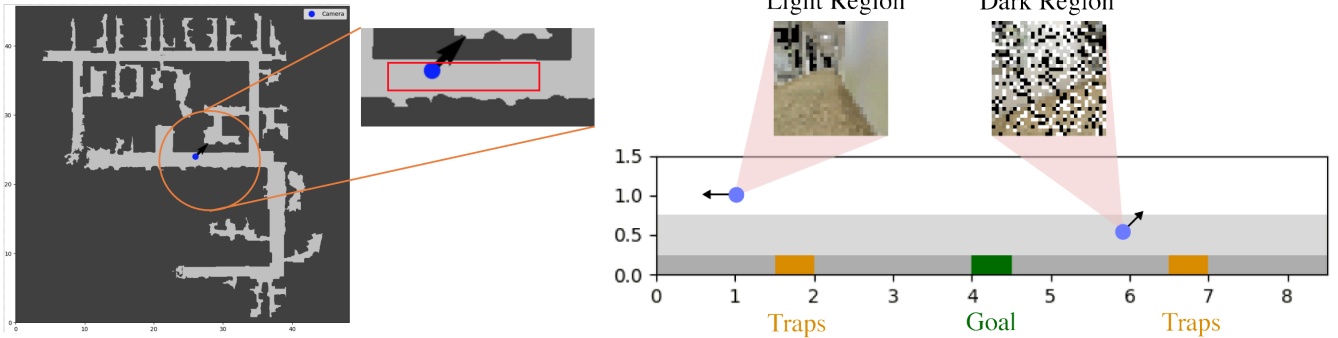


Figure 5: A top-down map of a floor in a building in the Stanford dataset (left). A visualization of the environment with the “trap” regions in orange and the goal region in green (right). The shaded part of the environment depicts the “dark” region, in which the image observations received by the agent are corrupted by salt-and-pepper noise. The rest of the environment is in the “light”, where the image observations are uncorrupted. The darkest gray region is a wall region that the agent cannot enter. The agent’s initial state is randomly chosen from a strip in the dark region.

ier observations in the dark region than the light region. The 3D Light-Dark problem extends this problem to have 3D image observations with salt-and-pepper pixel-wise noise. We used the Stanford building dataset (Armeni et al. 2017) to implement this problem structure, following similar specifications as (Wang et al. 2020). Fig. 5 shows a map of the environment with the agent depicted in blue. The agent’s location is given by (x, y, θ) , where x, y are the unknown absolute position coordinates and θ is the known heading. The observations consist of $32 \times 32 \times 3$ RGB images from the agent’s perspective. The agent receives a positive reward for reaching the goal and a negative reward if it enters a “trap”.

To train the Z_θ and P_ϕ models, we employed the following procedure. Each training batch consisted of random batches of samples $(s_t, \theta_t, o_t, \{\hat{s}_{t,i}\})$, where $s_t = (x_t, y_t)$. Here, θ_t was discretely chosen from $[0, 2\pi]$ at intervals of $\pi/4$. This is because the agent’s actions are in the form of headings and the planning algorithm that we use, PFT-DPW, works in a discrete action space. If s_t was in the dark region, then the $\{\hat{s}_{t,i}\}$ were generated from a normal distribution centered at s_t with standard deviation 0.1, and 0.01 for the light region. The difference in standard deviation was to enable the Z_θ and P_ϕ models to cause better localization in the light region than in the dark region. The two models were trained on a schedule that gradually introduced noise in the image observations o_t over the training epochs. In contrast, the generator G_ξ was trained simply with the random batches (s_t, θ_t, o_t) without the noise schedule, as if it were data collected by a randomly exploring agent. However, both sets of models could be trained either way in principle. For the generators, the concatenation of s_t and θ_t formed the conditional variable. We used a fully observable rollout for the tree search, as we found that yielded the best results.

Planner comparison. We compare the results from VTS and DualSMC in Table 1 for 500 testing episodes and averaged over 3 random seeds. Unlike the Floor Positioning problem, the training process for both algorithms occasion-

ally fails to converge, but the rate of this failure is low for both. Thus, we focused on quality rather than training stability by reporting results for 3 random seeds that succeeded.

In the Light-Dark problem and its variants, we see that VTS plans better than DualSMC not only by taking full advantage of the image features, but also by being able to adapt to different reward structures and distribution shifts in the noisy observations during test time. While VTS and DualSMC have comparable success rates, the VTS planner takes fewer steps to reach the goal. As illustrated in Fig. 6 (a), this is often because the VTS planner localizes better than the DualSMC planner and therefore does not need to take as many extra steps to travel into the light region.

This reveals important insights about where the difficulty lies in each problem. In the Floor Positioning problem, the challenge of de-localizing occurs since there is an inherent symmetry of the environment that causes degeneracy of observation. In particular, since the observations in the corridor states do not provide any information about which floor the agent is on, the particle proposer will propose particles in either of the floors. Without a recurrent component like LSTM in DualSMC that keeps track of encoded history, the agent will eventually suffer from de-localization without keeping the particle proposal scheme in check.

On the other hand, the main challenge in the Light-Dark problem is extracting information from image observations for proper localization. The VTS results show that the planner in fact is able to localize solely with the noisy observations in the dark region, which shows that while the salt-and-pepper noise observations are hard to interpret, they actually contain sufficient information to localize given enough observations. Thus, unlike the Floor Positioning problem, the agent will not easily suffer from de-localization as the observations give noisy but identifiable localization features.

Test-time changes to the environment. VTS has additional advantages in its robustness and adaptability, which we show through experiments on modified Light-Dark en-

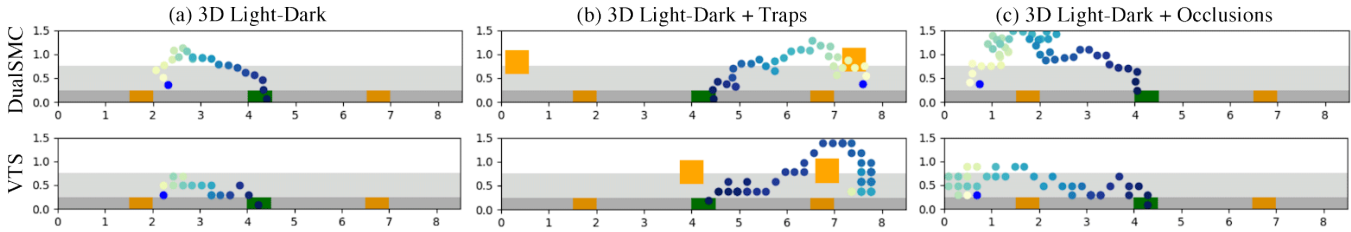


Figure 6: Example trajectories taken by DualSMC (top row) and VTS (bottom row) in three variants of the Light-Dark problem: (a) regular 3D Light-Dark problem, (b) 3D Light-Dark with variable traps, and (c) 3D Light-Dark with occlusions.

vironments. Since VTS uses an online planner, it can more easily adapt to new situations at test time without the need to retrain an entire planner. We also find that VTS is robust to distribution shifts in the image noise at test time.

In Table 1, we compare VTS and DualSMC when trap regions appear during test time that were not present during training. These regions could represent the presence of unforeseen obstacles or hazards. Over 500 testing episodes, we randomly generate the locations of two 0.5×0.5 square traps over a particular strip in the environment and compare the performances of the models trained over the 3 random seeds. We see in Fig. 6 (b) that while the DualSMC planner ignores these new trap regions because they are not represented by its models, the VTS planner is able to take into account rewards seen while planning. Thus, Table 1 shows that VTS achieves a much higher reward than DualSMC. VTS takes more steps because it tries to avoid these traps instead of taking its previous routes.

We also compare VTS and DualSMC when the form of the noise in the image observations changes during test time. Namely, during test time only, images seen in the dark region contain random blacked out occlusions instead of salt-and-pepper noise. Fig. 6 (c) additionally shows how VTS is able to maintain a good success rate and number of steps taken, while DualSMC struggles to generalize to this new scenario.

The additional robustness of VTS seems to be largely due to the Z_θ and P_ϕ models being trained with high fidelity data samples through random batch sampling or exploration, as opposed to on-policy training in DualSMC. The Z_θ and P_ϕ models in DualSMC are trained from an evolving replay buffer of tuples $(s_t, o_t, \{\hat{s}_{t,i}\})$, where the particle set $\{\hat{s}_{t,i}\}$ actually comes from the particle belief estimate inferred by DualSMC during training. This poses two layers of challenges for DualSMC: first, the state and consequently observation samples from the replay buffer end up being biased due to lack of control over on-policy exploration; second, the particle belief estimate in the dark regions often represent the de-localized belief state before proper localization. Thus, we conjecture that since the Z_θ and P_ϕ models in VTS receive higher fidelity data than those in DualSMC, the models in VTS learn more precise and robust features.

6 Conclusion

The development of the Visual Tree Search learning and planning algorithm suggests new ways to think about integrating learning and control and raises further questions

for researchers working in navigation and planning. VTS demonstrates that a more principled integration of control and planning techniques both illuminates the interpretability of each model component and saves training time by cleanly partitioning what each network is responsible for. This benefits researchers and practitioners alike, as a more interpretable and theoretically principled planner that is also quicker to train is beneficial in many practical scenarios where training resources are limited and the safety of a planner is important.

On the other hand, our work raises the question of what is the most natural, effective, and safety-ensured method of combining pre-existing controllers and planners, which are extensively studied both theoretically and experimentally, with learning-based components, which can model many complex functions and phenomena. VTS is one such way of accomplishing that goal, but there are other ways to achieve principled integration of learning and control.

Acknowledgments

This material is based upon work supported by a DARPA Assured Autonomy Grant, the SRC CONIX program, NSF CPS Frontiers, the ONR Embedded Humans MURI, Google-BAIR Commons, and the National Science Foundation Graduate Research Fellowship Program under Grant No. DGE 1752814. Any opinions, findings, and conclusions or recommendations expressed in this material are those of the authors and do not necessarily reflect the views of any aforementioned organizations.

References

- Alet, F.; Lozano-Perez, T.; and Kaelbling, L. P. 2018. Modular meta-learning. volume 87 of *PMLR*, 856–868. PMLR.
- Andreas, J.; Rohrbach, M.; Darrell, T.; and Klein, D. 2016. Neural Module Networks. In *IEEE CVPR*.
- Armeni, I.; Sax, A.; Zamir, A. R.; and Savarese, S. 2017. Joint 2D-3D-Semantic Data for Indoor Scene Understanding. *ArXiv e-prints*.
- Ayer, T.; Alagoz, O.; and Stout, N. K. 2012. A POMDP approach to personalize mammography screening decisions. *Operations Research*, 60(5): 1019–1034.
- Bai, H.; Cai, S.; Ye, N.; Hsu, D.; and Lee, W. S. 2015. Intention-Aware Online POMDP Planning for Autonomous Driving in a Crowd. In *IEEE ICRA*, 454–460. Seattle, WA, USA: IEEE.

Bertsekas, D. 2005. *Dynamic Programming and Optimal Control*. Massachusetts: Athena Scientific.

Browne, C. B.; Powley, E.; Whitehouse, D.; Lucas, S. M.; Cowling, P. I.; Rohlfshagen, P.; Tavener, S.; Perez, D.; Samothrakis, S.; and Colton, S. 2012. A Survey of Monte Carlo Tree Search Methods. *IEEE T-CIAIG*, 4(1): 1–43.

Corenflos, A.; Thornton, J.; Deligiannidis, G.; and Doucet, A. 2021. Differentiable Particle Filtering via Entropy-Regularized Optimal Transport. In Meila, M.; and Zhang, T., eds., *ICML*, volume 139 of *PMLR*, 2100–2111. PMLR.

Devin, C.; Gupta, A.; Darrell, T.; Abbeel, P.; and Levine, S. 2017. Learning modular neural network policies for multi-task and multi-robot transfer. In *IEEE ICRA*, 2169–2176. IEEE.

Garg, N. P.; Hsu, D.; and Lee, W. S. 2019. DESPOT- α : Online POMDP Planning With Large State And Observation Spaces. In *RSS*.

Gustafsson, F. 2010. Particle filter theory and practice with positioning applications. *IEEE Aerospace and Electronic Systems Magazine*, 25(7): 53–82.

Ha, D.; and Schmidhuber, J. 2018. Recurrent World Models Facilitate Policy Evolution. In *NeuRIPS*, 2451–2463. Curran Associates, Inc. <https://worldmodels.github.io>.

Hoerger, M.; and Kurniawati, H. 2020. An On-Line POMDP Solver for Continuous Observation Spaces. arXiv:2011.02076.

Holland, J. E.; Kochenderfer, M. J.; and Olson, W. A. 2013. Optimizing the Next Generation Collision Avoidance System for Safe, Suitable, and Acceptable Operational Performance. *Air Traffic Control Quarterly*, 21(3): 275–297.

Hudson, D. A.; and Manning, C. D. 2018. Compositional Attention Networks for Machine Reasoning. In *ICLR*.

Igl, M.; Zintgraf, L.; Le, T. A.; Wood, F.; and Whiteson, S. 2018. Deep Variational Reinforcement Learning for POMDPs. In Dy, J.; and Krause, A., eds., *ICML*, volume 80 of *PMLR*, 2117–2126. PMLR.

Jonschkowski, R.; Rastogi, D.; and Brock, O. 2018. Differentiable Particle Filters: End-to-End Learning with Algorithmic Priors. In *RSS*. Pittsburgh, Pennsylvania.

Kaelbling, L. P.; Littman, M. L.; and Cassandra, A. R. 1998. Planning and acting in partially observable stochastic domains. *Artificial Intelligence*, 101(1): 99 – 134.

Karkus, P.; Hsu, D.; and Lee, W. S. 2017. QMDP-Net: Deep Learning for Planning under Partial Observability. In Guyon, I.; Luxburg, U. V.; Bengio, S.; Wallach, H.; Fergus, R.; Vishwanathan, S.; and Garnett, R., eds., *NeuRIPS*, volume 30. Curran Associates, Inc.

Kirsch, L.; Kunze, J.; and Barber, D. 2018. Modular Networks: Learning to Decompose Neural Computation. In Bengio, S.; Wallach, H.; Larochelle, H.; Grauman, K.; Cesa-Bianchi, N.; and Garnett, R., eds., *NeuRIPS*, volume 31. Curran Associates, Inc.

Kochenderfer, M. J. 2015. *Decision Making Under Uncertainty: Theory and Application*. Massachusetts: MIT Press.

Kurniawati, H.; and Yadav, V. 2016. An online POMDP solver for uncertainty planning in dynamic environment. In *Robotics Research*, 611–629. Springer.

Lim, M. H.; Tomlin, C.; and Sunberg, Z. N. 2020. Sparse Tree Search Optimality Guarantees in POMDPs with Continuous Observation Spaces. In *IJCAI*, 4135–4142. International Joint Conferences on Artificial Intelligence, Inc.

Lim, M. H.; Tomlin, C. J.; and Sunberg, Z. N. 2021. Voronoi Progressive Widening: Efficient Online Solvers for Continuous State, Action, and Observation POMDPs. arXiv:2012.10140.

Mern, J.; Yildiz, A.; Sunberg, Z.; Mukerji, T.; and Kochenderfer, M. J. 2021. Bayesian optimized Monte Carlo planning. In *AAAI*. AAAI Press.

Meyerson, E.; and Miikkulainen, R. 2018. Beyond Shared Hierarchies: Deep Multitask Learning through Soft Layer Ordering. In *ICLR*.

Mirza, M.; and Osindero, S. 2014. Conditional Generative Adversarial Nets. arXiv:1411.1784.

Mittal, S.; Lamb, A.; Goyal, A.; Voleti, V.; Shanahan, M.; Lajoie, G.; Mozer, M.; and Bengio, Y. 2020. Learning to Combine Top-Down and Bottom-Up Signals in Recurrent Neural Networks with Attention over Modules. In *ICML*, volume 119 of *PMLR*, 6972–6986. PMLR.

Mnih, V.; Kavukcuoglu, K.; Silver, D.; Graves, A.; Antonoglou, I.; Wierstra, D.; and Riedmiller, M. 2013. Playing Atari With Deep Reinforcement Learning. In *NeuRIPS Deep Learning Workshop*.

Papadimitriou, C. H.; and Tsitsiklis, J. N. 1987. The Complexity of Markov Decision Processes. *Mathematics of Operations Research*, 12(3): 441–450.

Rosenbaum, C.; Klinger, T.; and Riemer, M. 2018. Routing Networks: Adaptive Selection of Non-Linear Functions for Multi-Task Learning. In *ICLR*.

Silver, D.; and Veness, J. 2010. Monte-Carlo Planning in Large POMDPs. In *NeuRIPS*, 2164–2172. Curran Associates, Inc.

Sohn, K.; Lee, H.; and Yan, X. 2015. Learning Structured Output Representation using Deep Conditional Generative Models. In Cortes, C.; Lawrence, N.; Lee, D.; Sugiyama, M.; and Garnett, R., eds., *NeuRIPS*, volume 28. Curran Associates, Inc.

Sunberg, Z.; and Kochenderfer, M. J. 2018. Online Algorithms for POMDPs with Continuous State, Action, and Observation Spaces. In *ICAPS*. Delft, Netherlands: AAAI Press.

Sunberg, Z. N.; Ho, C. J.; and Kochenderfer, M. J. 2017. The Value of Inferring the Internal State of Traffic Participants for Autonomous Freeway Driving. In *ACC*, 3004–3010. Seattle, WA, USA: IEEE.

Wang, Y.; Liu, B.; Wu, J.; Zhu, Y.; Du, S. S.; Fei-Fei, L.; and Tenenbaum, J. B. 2020. DualSMC: Tunneling Differentiable Filtering and Planning under Continuous POMDPs. In Bessiere, C., ed., *IJCAI*, 4190–4198. International Joint Conferences on Artificial Intelligence Organization.

Yang, R.; Xu, H.; Wu, Y.; and Wang, X. 2020. Multi-Task Reinforcement Learning with Soft Modularization. arXiv:2003.13661.

Ye, N.; Somani, A.; Hsu, D.; and Lee, W. S. 2017. DESPOT: Online POMDP Planning with Regularization. *Journal of Artificial Intelligence Research*, 58: 231–266.

Young, S.; Gašić, M.; Thomson, B.; and Williams, J. D. 2013. POMDP-based statistical spoken dialog systems: A review. *IEEE*, 101(5): 1160–1179.

Appendix

A Hyperparameters and Computation Details

Table 1 shows the hyperparameters used in training and filtering for VTS. Our models were trained on NVIDIA Tesla K80 GPUs. The hyperparameters for DualSMC training remained the same as the original work (Wang et al. 2020).

Table 1: Summary of hyperparameters used in training and filtering.

Hyperparameters	Floor Positioning	3D Light-Dark
Training gradient steps	500,000	100,000
Training sample pool size	-	16,000
Learning rate	0.001	0.0003
Batch size	64	64
Filtering particles	100	100
Percent of particles proposed	0.3	0.3
Resampling frequency	3	3

Table 2 shows the hyperparameters used for PFT-DPW planner. While hyperparameters for tree search planners are often chosen with hyperparameter sweeps and/or optimization, such meta-optimization in our algorithm would mean having to run our algorithm on a GPU numerous times, which was practically very inefficient. Thus, the hyperparameters were manually chosen via a combination of inspection and prior experience.

Table 2: Summary of hyperparameters used in PFT-DPW.

	n	c	k_a	α_a	k_o	α_o	m	H	γ
Floor Positioning									
	100	10.0	3.0	$\frac{1}{4}$	4.0	$\frac{1}{4}$	100	10	0.99
3D Light-Dark									
	100	10.0	3.0	$\frac{1}{4}$	4.0	$\frac{1}{4}$	100	10	0.99

Table 3 shows some parameters for the Floor Positioning and 3D Light-Dark environments. The environment parameters for Floor Positioning were left unchanged from Wang et al. (2020).

Table 3: Summary of environment parameters.

Hyperparameters	Floor Positioning	3D Light-Dark
Observation size	4	$32 \times 32 \times 3$
Agent velocity	0.05	0.2
Noise amount (image)	-	40%
Occlusion amount (image)	-	15×15

For the 3D Light-Dark problem, the Z_θ and P_ϕ modules were trained with a gradual noise schedule that was as follows: for the first 1/4 of the number of training epochs, the images in the training data had 0% noise. For the next 1/4 of the epochs, the images corresponding to states in the dark region had *final noise amount* * 1/4 percent noise. For the next 1/4 of the epochs, the images had *final noise amount* * 1/2 percent noise. For the final 1/4 of the epochs, the images had the full *final noise amount* percent noise. (As seen in Table 3, *final noise amount* was 40%.) This percentage corresponds to the percent of locations on the 32×32 image that were corrupted by the salt-and-pepper noise.

Finally, Table 4 shows the neural network architecture details for the Z, P, G models we trained on different experimental domains. We note here that although VTS and DualSMC differ in the architectures of their Z_θ and P_ϕ models in that the networks for VTS have deeper structures than those for DualSMC, we did not see any noticeable increase in performance for DualSMC with the deeper architectures in a preliminary exploration.

Table 4: Network details.

Model	Layers	# Channels
Floor Positioning		
Z_θ	5-layer MLP	$256 \times 3, 128, 16$
	Concat: state	18
	3-layer MLP	$256 \times 2, 1$
P_ϕ	3-layer MLP	$256 \times 2, 64$
	Concat: $z(64) \sim \mathcal{N}(0, 1)$	128
	4-layer MLP	$256 \times 3, 2$
G_ξ	Encoder	5-layer MLP
		$256 \times 4, 64$
		1 layer to output μ, σ
	Decoder	5-layer MLP
		$256 \times 4, 4$
3D Light-Dark		
Z_θ	Conv2d, filter (3, 3), stride 1	num image channels
	Conv2d $\times 4$, filter (3, 3), stride 2	32, 64, 128, 256
	Conv2d, filter (3, 3), stride 1	512
	3-layer MLP	1024, 512, 256
	Normalize output (*)	256
	3-layer MLP	256×3
	Concat: state, orientation	259
	4-layer MLP	$128 \times 3, 1$
P_ϕ	Same as Z_θ up to (*)	256
	1-layer MLP	256
	Concat: $z(256) \sim \mathcal{N}(0, 1)$, orientation	513
	3-layer MLP	$128 \times 2, 2$
G_ξ	Encoder	Same as Z_θ up to (*)
		256
		Concat: state, orientation
		259
	5-layer MLP	$256 \times 4, 128$
	1 layer MLP to output μ, σ	128
	Decoder	Concat $z(128) \sim \mathcal{N}(0, 1)$, state, orientation
		131
	5-layer MLP	256×5
	3-layer MLP	256, 512, 1024
	Conv2dTranspose $\times 3$, filter (3, 3), stride 2	128, 64, 32
	Conv2d, filter (3, 3), stride 2	num image channels